Active learning guided design and discovery of thermites with targeted properties

Leandro Carreira,[1] Claudia L. Ramírez,[1] Lea Pillemont,[1] Nicolas Richard,[2] Alain Esteve,[1] Matthieu Jonckheere,[1] and Carole Rossi[1]
[1)] *LAAS-CNRS, University of Toulouse, France*
[2)] *CEA-DAM, Bruyeres le Chatel, France*

(Dated: 18 March 2024)

This paper presents an active learning-based method designed to guide experiments or computations towards user-defined specific regions, termed "regions of interest," within vast and complex design spaces. The goal is to tailor material properties for target applications, especially in contexts where both experimentation and modeling pose challenges, as is often the case with energetic materials. We introduced a new acquisition function combining linearly two factors with the usual standard deviation of a Gaussian Process Regression algorithm. A first factor guides the sampling towards the defined zone of interest, and a second, is an incentive function that encourages the exploration of under-sampled regions of the design space. The motivation, rationale and expression of the proposed function are discussed in detail. Then, the practicality and effectiveness of our algorithm are illustrated through two distinct and important applications of Al/CuO reactive materials: thermal plugging and high-energy actions. We found that our algorithm effectively provides up several tens of thermites of interest well-distributed within the design space, after only 200 samplings, whereas, LHS procedure samples less than 10 points of interest. This research represents a significant advancement for large-scale problems in reactive materials science and engineering, where predicting the effect of feature modification is desired but limited simulations or experiments can be afforded due to their high cost.

I. INTRODUCTION

The influence of data science methods is experiencing rapid growth in materials science[1–4] and proves to be a powerful tool for systematically guide experiments or computations towards specific regions in vast and complex design space. Methods such as Bayezian optimization, classification, genetic algorithms have emerged as a efficient computational paradigm for extracting trends and patterns from large datasets[5–10]. In these approaches, data from both successful and failed experiments are used to train machine learning (ML) models. These models, in turn, predict whether a new data sample (not present in the training set) can exhibit properties superior to those in the training data. However, this improvement comes at the cost of extensive re-training procedures. These methods demonstrate great efficiency when a sufficient number of initial samples are available to train the surrogate. For instance, typical deep neural networks often require a substantial minimal volume of training data, typically ranging between 10^4 and 10^6 instances as discussed in[11]. Consequently, these models may not be suitable for case studies involving significantly smaller datasets (< 1000).

On the other hand, the discovery and optimization of materials still remains a significant challenge when dealing with a very large feature space (design space), limited data, and, if the experiments and/or calculations are expensive to perform. This is particularly relevant in reactive material design problems. Reactive materials are mixture of metallic fuel and oxidizer particles of around $10^2 - 10^4$ nm in size, that undergo an extremely high-temperature combustion (1000 – 6000 K range) and their burn rate and pressurization rate can be tuned in the ranges of $10^{-1} - 10^4$ m.s^{-1} and $1 - 400$ MPa.µs^{-1}, respectively, by adjusting the metal and oxide particle size, the metal purity, the powder density and the stoichiometry[12–17]. Exhaustive exploration of all these features space, denoted by $\mathbb{X} = \sum_i x_i$ to optimize some combustion property denoted by y_j is simply experimentally impossible and computationally demanding when using physics-driven models. A standard combustion tests typically performed to characterize the performance of a single reactive material configuration in a one-shot experiment, demands substantial quantities of material (at least tens of milligrams) and necessitates robust and costly safety measures. A few physical models[18–23] do exist but can not be applied for the generation of a large database as requested for ML models. The focus of this work is therefore to show how calculations from physical models can be guided optimally using active learning[24] to enable the sampling of Al/CuO reactive materials with targeted properties in as few iterations as possible to avoid the laborious unguided trial-and-error iterative process. The Al/CuO thermite was selected as reactive material as it is widely explored in various civilian and defense applications[25–28]. Additionally, physical models do exist to predict relationships between Al/CuO combustion properties (pressure and temperature) and material features, including the size of Al and CuO particles, the purity of Al, fuel-to-oxidizer stoichiometric ratio, as well as powder density[20,23,29,30].

A key element of our active learning approach involves training a Gaussian Process Regression[31] (GPR) as surrogate model to predict material properties while acknowledging the influence of uncertainties arising from statistical inference. This approach enables us to navigate the vast design space for materials, identifying those with superior properties compared to those present in the existing training dataset. Another central idea is that the surrogate model prediction efficiency should be optimized in zones termed as "of interest", where material properties are tailored for a particular application, rather than attempting to cover the entire feature space uniformly. To achieve this, within the GPR framework, we defined an acquisition function that enables a good tradeoff

between the quantity of interest based on physical inference (physical model) through an confidence bonus, and, the distance from the previous interesting point in the database to also guide the sampling to unexplored design spaces. This avoids to sample in very restricted zone of $\mathbb{X}$ and loose potential interesting points in unknown zones.

The contributions provided in this paper are threefold. First, we proposed a new acquisition function formed by combining different factors linearly with a GPR algorithm : 1) a first factor guides the sampling into a user-defined zone of interest, and, 2) an incentive function that encourages the exploration of under-sampled regions in the design space. Second, we demonstrate that the incentive function for coverage enhances the versatility of the optimization algorithm and enable to sample thermite materials in a wider part of the design space. This can be particularly useful to explore regions of the design space that are totally unknown by the user. Third, we demonstrate the efficiency of the proposed active learning process to identify Al/CuO thermites suitable for two distinct applications, thermal plugging and high energy actions.

II. METHODOLOGY AND COMPUTATIONAL DETAILS

This section provides the notations and basic concepts used all along the paper. We describe the mathematical formulations and give the computational details implemented in the proposed algorithms to efficiently explore the thermite design space, $\mathbb{X}$. The typical procedure consists of three major steps: first, m Al/CuO thermite configurations (training set) are sampled using the Latin Hypercube Sampling (LHS) to initialize the database (DB) and initiate the training of a surrogate. For each sample, the outputs (targets) in terms of combustion temperature (T_{max}) and pressure (P_f) are calculated using a physical model and define a given ground true value. Second, an approximation (surrogate) to the merit landscape of the design features is constructed using a GPR process. Third, a new set of features is proposed for the next predictions based on a sampling strategy defined by an acquisition function, seeking to strike a balance between DB exploration and exploitation (quantity of interest based on physical inference).

A. Physical model: ground truth values

A physical simulator of the Al/CuO thermite combustion was used to calculate T_{max} and P_f, the two targets, as a function of Al and CuO microstructure data (termed as features). Full details about the model from its physico-chemical foundations and numerical implementation can be found in ref.[23].

In this current work, we focus on only three features among a dozen, the Al and CuO particles radius, noted as r_{Al} and r_{CuO} respectively, and the Al over CuO molar ratio, or Al richness, noted as ϕ. The range of r_{Al}, r_{CuO} and ϕ values are given in Table II A corresponding to technological constraints.

TABLE I. Description of the features and targets with their range of variation (design space $\mathbb{X}$ considered in this work)

Variables	Description	Range
r_{Al}	Aluminum particle radius	0.1 - 10 µm
r_{CuO}	Copper oxide particle radius	0.1 - 10 µm
ϕ	Aluminum richness	1 - 4
T_{max}	Combustion temperature	600 - 7500 K
P_f	Gas pressure	0.2 - 150 MPa

B. Latin Hypercube Sampling

LHS is a systematic and efficient sampling technique dedicated to multiple dimensional problems in statistical studies and simulations. In contrast to uniform random sampling methods, which are susceptible to the concentration of distance effects, LHS ensures a well-distributed representation of values across the design space, offers potentially improved coverage, and, reduces the chances of overlooking parameter areas. In addition to initialization, LHS is employed as a benchmark algorithm to assess the active learning algorithm proposed in this study.

C. Review of Gaussian Process Regression

Gaussian process regression[31] is used to construct the surrogate for the objective function. Briefly, mathematically, we posit that given the input x, the output Y_x seen as a random variable can be expressed as $Y_x = g(x) + \varepsilon$, where ε is a Gaussian noise, and $g : \mathbb{R}^D \to \mathbb{R}^d$, with D the number of features (3 in our case) and d the number of targets of the model (2 in our case). More precisely, the GPR model assumes a prior distribution over each sample in the design space, represented by a mean function $\mu(\cdot)$ and a covariance function $k_\theta(\cdot,\cdot)$, also called kernel. μ represents the value of g, while the kernel captures the similarity or correlation between input points and thus significantly influences the predictions efficiency[31]. Various types of kernels are used in practice, including the constant, linear, squared exponential (RBF), Matérn, white noise, and more. The package for GPR on Scikit-Learn[32] was employed with the RationalQuadratic kernel and the default values for their parameters, except for the *length_scale _bounds*, with a range of $[10^{-7} - 10^5]$.

From a learning perspective, GPR is a probabilistic regression model, utilizing a training dataset to approximate the posterior distribution for each target, y. With the initial set of training samples $(x_i, y_i)_{1\leq i\leq m}$, the goal is to achieve generalization to unknown data by making predictions while estimating the associated uncertainty, quantified through the variance of the GPR at each point. In subsequent discussions, the notation $FIT_{GP}((x_i, y_i)_{1\leq i\leq m})$ is employed to represent the optimization step for determining the best weights θ_m of the GPR. $\hat{g}$ denotes the GPR approximation of the function g. Noteworthy, unlike many other learning algorithms, one of the significant advantages of the GPR is their ability to offer transparent quantification of uncertainty, achieved through estimates of

standard deviations. For constructing the GPR surrogate, we employed the features presented in Table II A and considered the P_f and/or T_{max}, as targets y.

D. Multistage sampling strategy based on active learning

Active learning is a paradigm within supervised machine learning that optimizes prediction accuracy with a reduced number of training samples. It achieves this by iteratively training a predictor (surrogate) and utilizing the predictor in each iteration to select training examples that contribute the most to accuracy improvement. Numerous recent research endeavors have concentrated on refining acquisition functions for GPR across various application domains, as exemplified by[33,34].

Thus the optimization results are incrementally improved by interleaving exploration and exploitation steps. We implemented this methodology to ensure a thorough exploration of the design space and avoid getting stuck in local minima, which might limit the discovery of optimal material properties.

The sampling strategy is therefore defined through one acquisition function $F_{\theta_k}(\cdot)$ seeking to obtain a balanced sampling by considering a trade-off between exploring the *unknown* areas of $\mathbb{X}$ (where the standard deviation is highest), and exploiting the areas where a good outcome (T_{max} and P_f) is known (defined as region of interest).

$$F_{\theta_k}(u) = \bar{\sigma}_{\theta_k}(u) + I_{\theta_k}(u) + C_{s,d,A}(u) \tag{1}$$

where

$$\bar{\sigma}_{\theta_k}(u) = \frac{\sigma_{\theta_k}(u)}{M_{\theta_k}}, \tag{2}$$

where σ_{θ_k} is the standard deviation (STD) of the surrogate (given by the GPR) and M_{θ_k} is an estimation of $\max_x \sigma_{\theta_k}(x)$. Consequently, the $\bar{\sigma}_{\theta_k}$ function always yields a value between 0 and 1, besides the standard deviation of the surrogate getting smaller as the training procedure advances.

Considering that STD can be influenced by outliers or unexplored regions outside the intended scope of interest, potentially exerting undue influence on the selection process, we have introduced a function I, acting as a selective filter on the region of interest. This addition aims to mitigate the impact of these values in the optimization algorithm, thereby guiding the sampling into the user-defined zone of interest for a more accurate and robust selection process. We hence define the I function as the probability (given by the current GPR process prediction) of a point u falling inside the zone of interest:

$$I_{\theta_k}(u) = P\left(\hat{g}_{\theta_k}(u) \in [L,U]\right) \tag{3}$$

where L and U are the lower and upper bounds of each zone of interest (and have the same dimensionality d as the output y).

The function I approaches unity when the d-dimensional Gaussian distribution is predominantly contained within the boundaries of the regions of interest, and tends toward zero when only the tail of the distribution extends into these regions. It significantly capitalizes on already explored areas within the region of interest.

Let us now describe the function $C_{s,d}$ which serves as an incentive function for exploration, fostering the exploration of under-sampled regions within the domain $\mathbb{X}$.

$$C_{s,d,A}(u) = 1 - \frac{1}{1+\exp(A - s\,\Gamma_d(u))} \tag{4}$$

with

$$\Gamma_d(u) = \sum_{x \in \mathbb{X}_k} \exp\left(-d\,\|u-x\|_2\right) \tag{5}$$

where $x \in \mathbb{X}_k$ are the already explored points, d is a decay parameter to penalize points very close to the already explored points, s is the Sigmoid parameter that controls the speed of the function, and 5 is a constant that translates the Sigmoid horizontally so this function is close to zero when the sum of distances $\Gamma_d(u)$ is close to zero.

Physics indications regarding the typical scale of the design spaces guide our selection of the parameters A, s, and d. Specifically, we fixed $A = 5$ to ensure that the sigmoid function approaches values close to zero when its input equals zero. The decay parameter d and the sigmoid speed parameter s vary within the ranges of 18 to 25 and 3 to 10, respectively. Parameter d governs the proximity threshold for nearby points, with larger values restricting consideration to only very close points. Conversely, parameter s determines the tolerance for closeness, with smaller values allowing a greater number of points to be considered close before incurring significant penalties

To gain deeper insights into the individual contributions of the components within $F_{\theta_k}(u)$, we conducted experiments by selectively disabling each term. Specifically, we examined the following variations:

$$F^{(1)}_{\theta_k}(u) = I_{\theta_k}(u) \tag{6}$$

$$F^{(2)}_{\theta_k}(u) = \bar{\sigma}_{\theta_k}(u) + I_{\theta_k}(u) \tag{7}$$

This approach allowed us to evaluate the isolated effects of each term and compare them against the complete results in Table II.

E. Active learning workflow and algorithm

We evaluated the acquisition function based on the characteristics of the data and the predictions made by the GPR model. Concretely, the multi-stage sampling strategy can be divided into several consecutive steps.

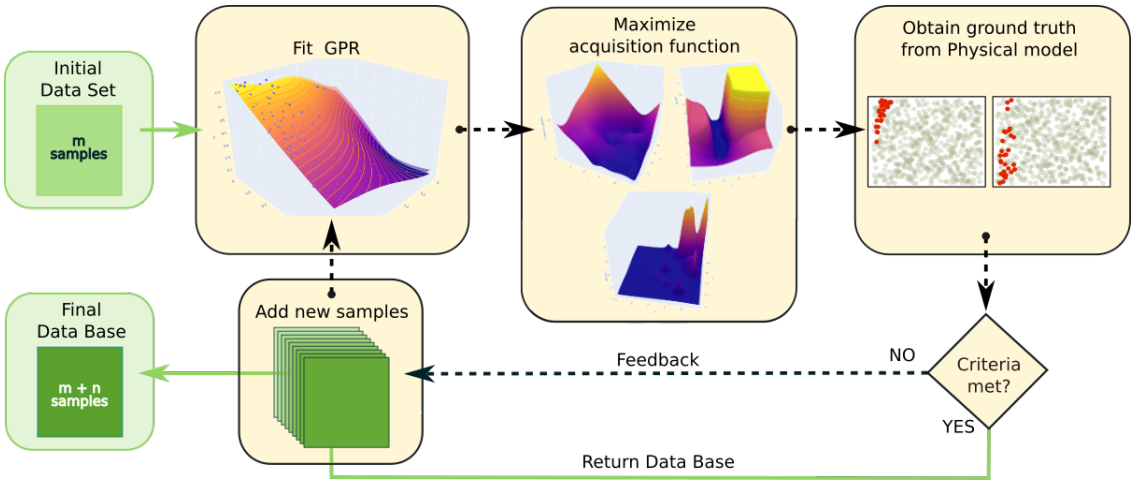

FIG. 1. Schematic of the active learning strategy algorithm. An initial dataset with m points is built to initiate the training of the surrogate by fitting the GPR. Then, the acquisition function is optimized to obtain a set of sample candidates to explore. The ground truth of each candidate is calculated through the physical model, fitting again the surrogate model to obtain a new predictive distribution. The dotted black line represents the loop responsible for constructing the database, which halts based on criteria such as no improvement or reaching the maximum budget, and then returns the constructed database.

- **Preparation of system.** The user specifies a domain of interest for the targets $T_{\max}$ and P_f, which characterize the desired combustion properties for the chosen application. A thermite that yields the desired combustion properties within this user-defined region is referred to as a point of interest. Next, all variables (Table II A) are scaled between 0 and 1, to help the algorithm to achieve better and faster results. The user also enters the exploration parameters s and d, for function $C_{s,d}$.

- **Initialisation of the database and surrogate.** A training set of 100 points (m) is sampled in the design space $\mathbb{X}$ by LHS to train the surrogate.

- **Activation of the active learning method.** We then activate each term of the acquisition function, E, I or $C_{s,d}$, independently or coupled, to sample the design space $\mathbb{X}$. 200 samplings is the limit set in this work due to the difficulty and expense of experimenting with energetic materials. It is important to mention that at each iteration, we sample 7 points simultaneously and execute the physical simulator in parallel to maximize efficiency. Subsequently, we select the top 7 candidates with the lowest values to minimize $F_{\theta_{t-1}}(u)$, and conduct their corresponding experiments in parallel, with one experiment per available CPU. Hence, 200 samplings represent approximately 30 iterations of the algorithm.

- **Data analysis.** For the analysis, we constructed a database comprising 300 sampled points. This includes 100 points from the training set and additional 200 points sampled using the active learning algorithm.

The algorithm of this methodology is given below.

Algorithm 1 Active Learning

Require: $I_R, (x_i, y_i)_{i\leq m} \in \mathbb{X}$
  scale $\mathbb{X} \to \mathbb{X}_{[0,1]}$
  compute $\theta_m, \hat{g} \leftarrow FIT_{GP}((x_i, y_i)_{i\leq m})$
  for $t \leftarrow m+1$ to n **do**
    $x_t \leftarrow MIN\left[F_{\theta_{t-1}}(u)\right]_{\{u\in\mathbb{X}_{[0,1]}\}}$
    $y_t \leftarrow g(x_t)$
    $\theta_t, \hat{g} \leftarrow FIT_{GP}((x_i, y_i)_{i\leq m+t})$
  end for ▷ **return** $(x_i, y_i)_{i\leq m+n}$

III. RESULTS AND DISCUSSION

The developed active learning strategy is analyzed and discussed through the exploration of two target applications: thermal plugging and high-actuation such as pyro-fuzing[35]. For welding applications, the motivation is to design Al/CuO thermites that generate combustion temperatures and pressures in the range 2000-4500 K and 1 - 2 MPa, respectively. These specified Temperature-Pressure values define the region of interest 1 (referred to as R1) for the exploration. The second application requires very high pressure and temperature, i.e., in the range of 40-56 MPa 5800-7000 K, respectively. These specified Temperature-Pressure values define the region of interest 2 (R2).

As a mean to get a reference estimate of both regions 1 and 2, we ran 19404 simulations using the brute force LHS technique. Figure 2 depicts the spatial distribution of the thermites of interest (red balls) within the domain $\mathbb{X}$ (Table II A) corresponding to the region R1 (a) and region R2 (b). The 653 thermites of interest for welding applications exhibit specific characteristics : the aluminum radius is constrained to be below 3 µm, while the copper oxide radius can span the entire range [100 nm - 10 µm]. The richness falls within the range of 1.2 to 4, with a denser spread of samples as the richness

increases. Reducing the richness involves decreasing the aluminum radius to below 1 μm. Now, analysing the Figure 2(b), we see that 988 thermites can produce high pressures and high temperatures as specified by region of interest 2. It is interesting to note that their characteristics are totally different from those of thermites suitable for welding. Both the aluminum and oxide radius are microscopic, and the aluminum richness must remain below 1.5.

A. Sampling Al/CuO thermite materials for thermal-plugging application

In this section, we evaluate the efficiency of our algorithm in guiding the sampling process to effectively identify a significant number of thermites of interest from the pool of 653 options. Our aim is to achieve the best possible spatial distribution of these points across the design space. One primary metric for assessing efficiency is therefore the ratio of sampled points of interest over the total number of sampled points, followed by visualization and quantification of the spatial spreading of the guided exploration. Three different sampling scenarii were analyzed :

- *Scenario 1. Activation of the interest term I (I-only).* We activate the term I of the acquisition function without considering the STD value of the GPR. In that case, the choice of a new point in the database is only driven by the criteria to fall into the region of interest defined by the user.

- *Scenario 2. Activation of E and I terms (GPR+I).* We consider both, STD value of the GPR which provides iterative exploration directions based on the standard deviation and also activate the term I of the acquisition function to reward points that fall into the region of interest.

- *Scenario 3. Activation of all terms, E, I and $C_{s,d}$ (GPR+I+C).* In a last scenario, we activate all terms of the acquisition function to guide the sampling toward zone of interest while exploring a wide domain of the design space. We set $d = 20$ for the decay and $s = 5$ for the Sigmoid speed.

Table II summarizes the number of points of interest (in #) that are sampled when increasing the database by batches of 100 samples. The percentages of points of interest relative to the total sampled points (in %) are highlighted in italics. LHS as a non iterative procedure is provided for comparison purposes.

Sampling 200 points using the non-iterative LHS method does not show remarkable progression in the number of points being collected within the region of interest. Starting at 5% of interesting points within the 100 points of the training set, the ratio slightly increases to ∼7% upon doubling the sampling and then stagnates around ∼6.3%. This indicates that no additional specific region of interest emerges from this uniform sampling.

TABLE II. Evolution of the number of points of interest (in #) and their ratio in % over the total number of sampled points (in italics) calculated after each increment of 100 additional points. Region of interest, R1, is defined for temperatures and pressures in the range 2000-4500 K and 1-2 MPa, respectively.

Added	**LHS**		**I-only**		**GPR+I**		**GPR+I+C**	
points	in #	*in %*	in #	*in %*	in #	*in %*	in #	*in %*
0	5	*5.0*	5	*5.0*	5	*5.0*	5	*5.0*
100	14	*7.0*	101	*50.5*	71	*35.5*	63	*31.5*
200	19	*6.3*	200	*66.7*	149	*49.7*	134	*44.7*

This is confirmed by examining the spatial distribution of sampled points, which includes the 200 points from Table II along with the 100 points from the training set. These points are projected onto the three feature scales (r_{CuO}, r_{Al}, and ϕ), as shown in Figure 3. Red balls correspond to points of interest, while gray balls represent non-interesting points. Through LHS sampling, nine interesting points are identified, evenly distributed across the three feature dimensions. Notably, no interesting point was found for $\phi < 3$.

When utilizing solely I for guiding the sampling process (I-only column of Table II), a considerable improvement in sampling efficacy towards points of interest is observed. Out of the 300 sampled points, 67% are of interest, in contrast to only 6.3% using the uniform sampling method. However, their spatial distribution show clustering propensity. Indeed, the bright red balls in Figure 3 (column I) indicate that many sampled points are in close proximity to each other, particularly evident in the ϕ-r_{CuO} plane. The sampled points of interest are concentrated in zones characterized by $r_{CuO} < 6$ μm, $r_{Al} < 2$ μm and $\phi < 2$. This clustering demonstrates the limitation of relying solely on I function for guiding the process.

Activating E+I in the acquisition function enables consideration of the standard deviation amplitude when selecting new samples, providing a method to spread exploration towards less defined regions. As summarized in the GPR+I column of Table II, we still observe an enhancement of the sampling efficiency towards the region of interest compared to LHS. Out of the 300 sampled points, 49.7% are of interest, compared to only 6.3% using the uniform sampling method. While the efficiency in collecting points of interest is slightly less significant compared to the I-only strategy, interestingly, the clustering effect is now less pronounced (Figure 3, column GPR+I). The spatial distribution of the region of interest extends towards low richness ($\phi < 2$), particularly visible on the ϕ-r_{CuO} and ϕ-r_{Al} planes. This is attributed to the consideration of STD, which guides the sampling towards unpopulated zones of the design space, where the surrogate is farther from the true function. However, we do not sample much thermites featuring a $\phi > 3$ and $r_{CuO} > 6$ μm whereas many points of interest are present in the upper part of the ϕ-r_{CuO} plane of Figure 2(a).

Now, activating the incentive component $C_{s,d}$ of the acquisition function modestly enhances spatial distribution of the sampled points of interest (Figure 3, 2D diagrams corresponding to GPR+I+C versus GPR+I). We distinguish some new points of interest for large CuO radius, typically r_{CuO} = 10

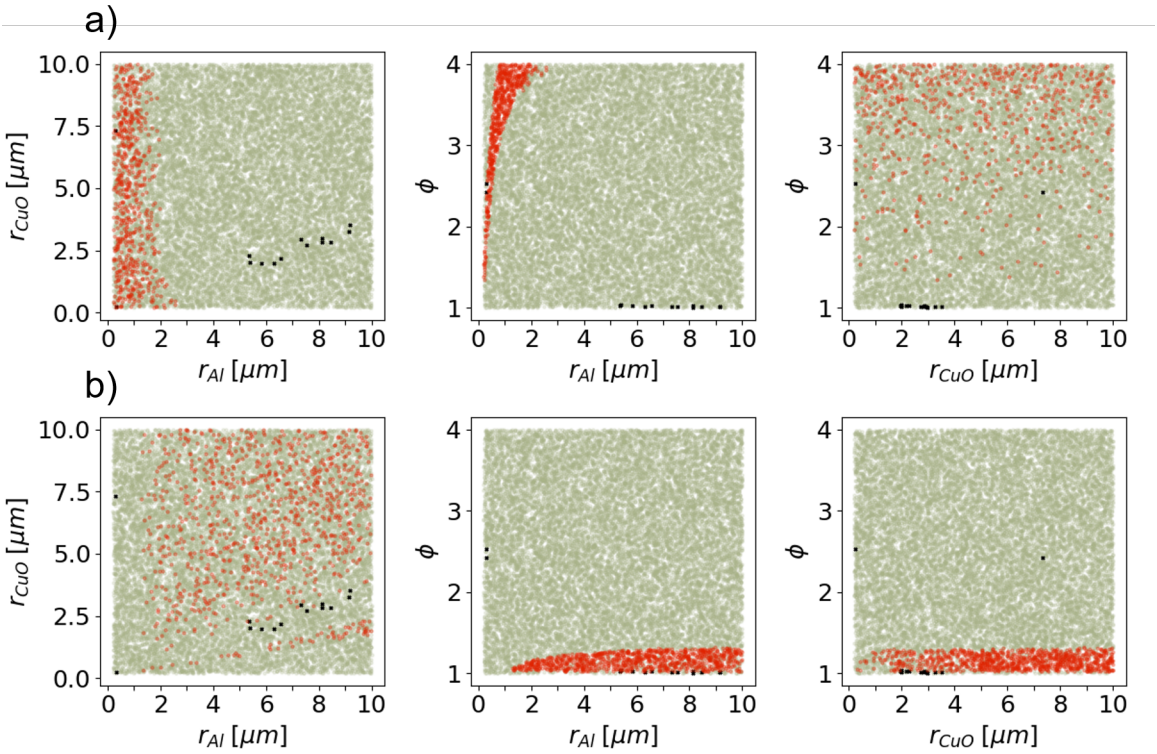

FIG. 2. Spatial distribution of points of interest (red balls) within the design space $\mathbb{X}$, obtained employing LHS projected onto main feature scale planes. a): region of interest, R1 (653 points of interest); b) region of interest, R2 (988 points of interest). Gray balls represent non-interesting points, and black crosses indicate outliers (out of the range, 14 points). The total number of sampled points is 19404.

μm and $2 < \phi < 3$. The effect of the coverage function is slightly noticeable in the ϕ-r_{CuO} plane. To further quantify the coverage of the design space, and thus assess the effectiveness of the $C_{s,d}$ function in facilitating the exploration of under-sampled regions within the domain $\mathbb{X}$, we calculate the volume occupied by points of interest within the 3D-domain space for each strategy. To achieve this, we create mesh spheres centered at each sampled point, outlining the region deemed unnecessary for sampling a new point. A radius of 0.025 is chosen, indicating that for a sampled point to be considered interesting (i.e., not too close to a point already in the database), its three features—r_{CuO}, r_{Al}, and ϕ—must vary by less than 2.5%. The total volume occupied by points of interest was computed using the Vedo library, a Python module designed for the scientific analysis of 3D objects and point clouds. This library is built upon VTK and numpy[36].

If the distance between spheres is greater than the diameter of a sphere, indicating that the spheres are well separated, we sum their volumes. However, in cases where the distance between two spheres is less than the diameter of a sphere, indicating intersection, we compute the volume of the intersecting spheres by utilizing the capability of performing boolean operations between meshes in the Vedo library. Then, by merging the intersecting spheres into a single mesh and subsequently invoking the ".volume" method of the Vedo meshes, we determine their respective volumes.

The sum of all volumes divided by the number of points provides a comprehensive representation of the total explored volume. Results are reported in Table III.

The results show that when the incentive function is activated (column GPR+I+C), the total volume of the design space that is covered by the points of interest is equal to 1.76×10^{-5}, two times those computed with the GPR+I strategy being of 8.8×10^{-6}. This confirms that the design domain is much better covered when part $C_{s,d}$ of the acquisition function is activated. The total volume of the design space covered by points of interest sampled using I-only strategy is only 6.27×10^{-6} despite discovering a larger number of points of interest, confirming that a significant proportion of those points are closely clustered. This result undoubtedly underscores that GPR+I+C surpasses all other methods. When the sampling is guided by LHS, expectantly, the volume of the region of interest per point remains constant 4×10^{-6}.

As a final analysis, we present violin and Kernel Density Estimate (KDE) plots (Figures 4 and 5) detailing the distribution of the target values (P_f, T_{max}) of the 300 Al/CuO thermites contained in each database (100 training points + 200 points sampled by each strategy).

Analyzing the violin plots, we observe that the final pressure target of the database generated with LHS (gray) reveals an unimodal distribution slightly above the region of interest. This distribution appears compressed both below and above this specific region. In contrast, for the combustion tempera-

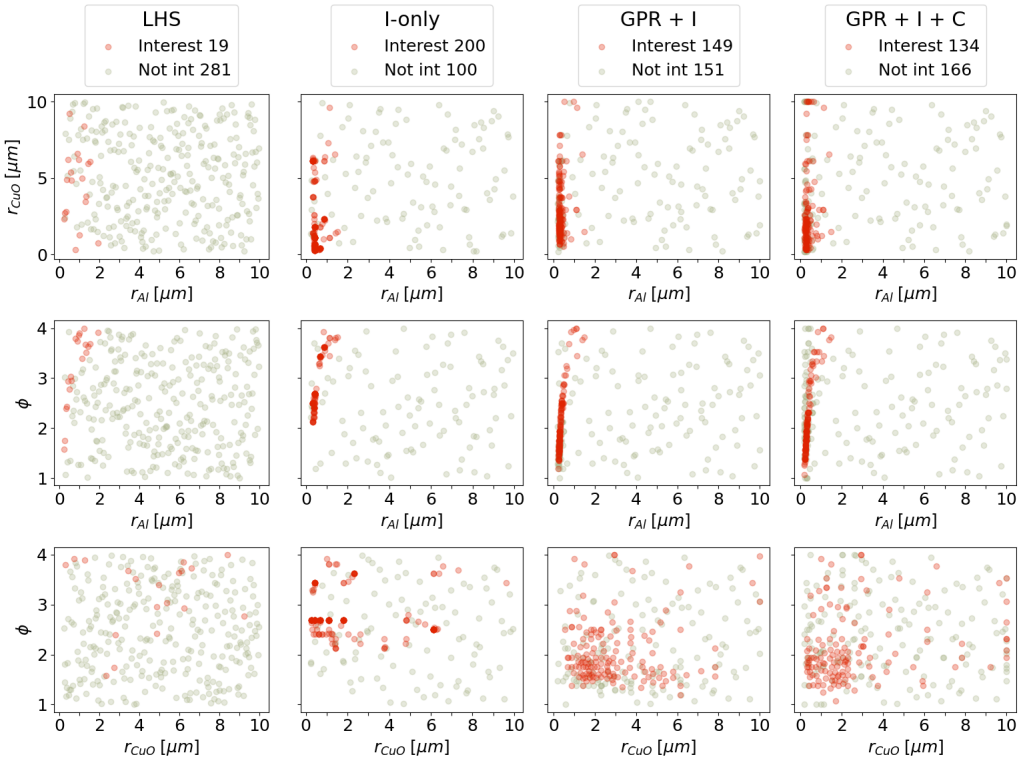

FIG. 3. Spatial distribution of the total number of sampled points (300) projected onto main feature scale planes. Red balls correspond to points of interest, while gray balls represent non-interesting points. Region of interest, R1, is defined for temperatures and pressures in the range 2000-4500 K and 1-2 MPa, respectively. "Not int" *stands for not interesting points.*

TABLE III. Volume of region of interest divided by number of points (Vol Int) considering a database of 100 and 200 sampled points. The computation of the volume involves the creation of spheres, each centered at a feature point within a sampled 3D space constrained to the [0, 1]^3 range (the scaled feature space), each with a fixed radius of 0.025. The overlapping volume is computed using a boolean union operation and subtracted to the total volume.

Added	**LHS**		**I-only**		**GPR+I**		**GPR+I+C**	
points	Vol Int	Vol Tot	Vol Int	Vol Tot	Vol Int	Vol Tot	Vol Int	Vol Tot
100	4.40×10^{-6}	6.49×10^{-5}	8.2×10^{-6}	4.05×10^{-5}	1.81×10^{-5}	5.5×10^{-5}	1.91×10^{-5}	6.25×10^{-5}
200	4.02×10^{-6}	6.44×10^{-5}	6.27×10^{-6}	2.78×10^{-5}	8.8×10^{-6}	3.6×10^{-5}	1.76×10^{-5}	5.16×10^{-5}

ture, the distribution is predominantly situated above the region of interest, with a narrow distribution located within that area. Guiding sampling with I-only strategy (yellow), we observe a more distributed shape centered within the zone of interest. While this leads to a higher concentration of samples within the region of interest, the distribution for the combustion temperature is primarily centered around 3500 K. Upon applying the GPR+I and GPR+I+C strategies, the distribution of both targets undergoes a much more distributed shape within the zone of interest confirming the effectiveness of the exploration strategy.

This conclusion is confirmed in KDE plots (Figure 5) where the region of interest is delineated by red vertical lines. The increased density of points in the region of interest is clearly visible when using the GPR+I+C strategy compared to GPR+I one, which was more difficult to appreciate from the violin plots.

As a summary of this first section, among the 653 interesting thermites suitable for welding applications, GPR+I+C quickly identifies 63 points of interest after only 100 iterations. Interestingly, the resulting database is homogeneously distributed across the 3D design space $\mathbb{X}$, as the algorithm found points of interest with Al and CuO radius spanning the entire range [0.1 - 10 µm] and $1.2 < \phi < 3$. This underscores the effectiveness of the active learning strategy, although sampling is defective in region characterized by $\phi > 3$ and $r_{CuO} >$ 6 µm.

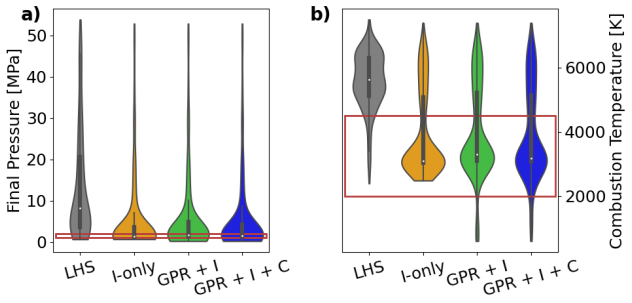

FIG. 4. Violin plots depicting the targets of the 300 Al/CuO sampled thermites obtained with LHS and each active sampling scenario. a) Final pressure, b) Combustion temperature. The red lines mark the limits of the region of interest R1.

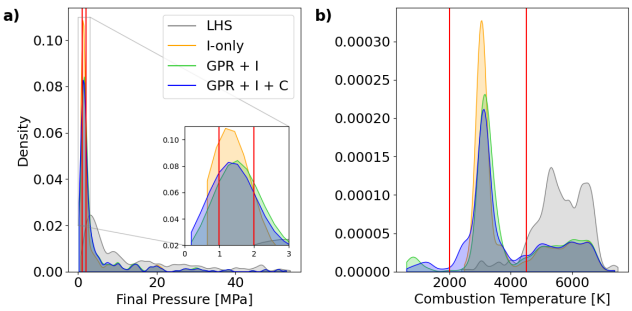

FIG. 5. KDE plots depicting the targets of the 300 Al/CuO sampled thermites obtained with LHS and each active sampling scenario. a) Final pressure, b) Combustion temperature. The red lines mark the limits of the region of interest R1.

B. Database of Al/CuO thermite materials for actuation application

In this final section, we evaluate the efficiency of our algorithm in guiding the sampling process to identify a reasonable number of thermites of interest from the pool of 988, ensuring their uniform distribution within the design space. We follow the same sampling procedure as described in the previous section, exploring three scenarios. We discuss the results for only the two strategies, GPR+I and GPR+I+C, in comparison with LHS sampling. It has to be noted that within the specified second region of interest, the temperature and pressure range are both extremely high and narrow. To generate such extreme Pressure-Temperature characteristics during Al/CuO combustion, a low Al over CuO mass ratio (ϕ) is necessary (Figure 2) as discussed in ref.[37,38]. Excess CuO allows for the generation of oxygen species in the gas phase, contributing to pressure. However, achieving temperatures of 5800 - 7000 K also requires a sufficient quantity of Al, the fuel, to produce heat. A delicate balance must be struck. Consequently, sampling interesting points and achieving a sufficient coverage with only 200 points may pose a challenge.

Table IV presents the number of points of interest falling into R2 region and their ratio over the total number of sampled points calculated after each increment of 100 additional points.

TABLE IV. Evolution of the number of points of interest (in #) and their ratio in % over the total number of sampled points (in italics) calculated after each increment of 100 additional points. Region of interest, R2, is defined for temperatures and pressures in the range 40-56 MPa and 5800-7000 K, respectively

Added	**LHS**		**GPR+I**		**GPR+I+C**	
points	in #	*in %*	in #	*in %*	in #	*in %*
0	5	*5.0*	5	*5.0*	5	*5.0*
100	10	*5.0*	43	*21.5*	21	*10.5*
200	18	*6.0*	88	*29.3*	30	*10.0*

The non-iterative LHS method is totally ineffective in such delicate situation: only 18 interesting points out of 200 samplings are found (6%). They are widely spread across the design space (Figure 6). Activating *E+I* in the acquisition function (GPR+I column of Table IV), we observe an effective enhancement of the sampling efficiency towards the region of interest compared to LHS. 88 interesting points are found (approximately 30%) compared to only 6% using LHS. But among the 88 points, a large majority (approximately 90%) are concentrated in a very narrow zone of the design space: ϕ = 1.2 and r_{CuO} and r_{Al} in the range of [2 - 2.5 µm] (Figure 6, column GPR+I). This outcome is consequently uninteresting for the user who prefers to obtain fewer points but with features well spread across the technological range, enabling him/her to make a choice based on other constraints. Activating the incentive component $C_{s,d}$ of the acquisition function enhances spatial distribution of the sampled points of interest (Figure 6, 2D diagrams corresponding to GPR+I+C versus GPR+I) while reducing the efficiency of sampling into the region of interest. Only 30 interesting points are found (10%) after 200 points, but their features are interestingly well spread in the design space. The user can select Al/CuO thermites with r_{CuO} and r_{Al} spanning almost entire range [0.5 µm - 10 µm] defined in the specifications (Table II A). This represents a highly significant and advantageous capability.

Now examining the violin plots (Figure 7) of the targets of the database formed by the 300 sampled points, it becomes apparent that reaching the final pressure target is challenging even when guiding the sampling. We do observe a slight bump on the Pressure distribution when sampling is guided (green plot), but it remains relatively subtle. This is because we do not allow ϕ to be lower than 1, which is required to produce extremely high pressure. In contrast, reaching the final temperature target is less challenging, as the database generated using GPR+I and GPR+I+C exhibits a well-distributed shape centered around [5800 - 7000 K]. Interestingly, the database generated using only LHS (gray) exhibits both targets outside the region of interest, which was expected as only 6% of points fall within the defined Pressure-Temperature region.

These observations are confirmed with more detail in KDE plots (Figure 8) where the region of interest is delineated by red vertical lines. The increased density of interesting points in the region of interest is clearly visible when using

the GPR+I strategy compared to GPR+I one, which was concluded from results of Table IV.

Finally, we also computed the design space coverage to quantify the effectiveness of $C_{s,d}$ using the method of the sphere previously described. The results confirm the findings, i.e better coverage of interesting points: the total volume of the design space occupied by points of interest sampled using GPR+I+C is 5 times greater than those sampled using GPR+I alone, 5.1×10^{-6} versus 1.31×10^{-6}.

IV. CONCLUSION

This work has introduced an active learning strategy for selecting optimized Al/CuO samples in the vast 3D-design space, *i.e.*, materials with properties falling within a specific user-defined range of interest. We used an acquisition function combining two factors linearly with the STD of a GPR algorithm: 1) a factor, I, that guides the sampling into the user-defined zone of interest, and, 2) an incentive function that encourages the exploration of under-sampled regions in the design space. Out of the 653 thermites suitable for welding applications within the design space, our algorithm rapidly identifies 63 interesting points after just 100 iterations. This number increases to 134 after 200 samplings, against only 19 points identified using an uniform sampling procedure. Regarding the second application, high-energy actions, although finding thermites capable of generating extreme pressure and temperature simultaneously is highly challenging, our optimization algorithm succeeded in rapidly identifying 21 interesting points well-spread in the design space, after only 100 iterations. This number increased to 30 after 200 samplings, compared to only 18 points identified using a uniform sampling procedure. Clearly, the results of this study proves the effectiveness, robustness and accuracy of our optimization algorithm to guide thermites sampling towards user-defined zones. It also demonstrated the crucial role of the incentive function in preventing the selection of thermites in highly restricted zones of $\mathbb{X}$. This research represents a huge progress for large-scale problems in material science and engineering, beyond reactive material design, where we desire to predict the effect of feature modification but can only afford a limited number of simulations or experiments due to their very expensive cost.

ACKNOWLEDGMENTS

This work was primarily funded by the European Research Council (ERC) under the European Union's Horizon 2020 research and innovation program (grand agreement No. 832889 - PyroSafe).

V. REFERENCES

[1]J. J. de Pablo, B. Jones, L. K. Cora, V. Ozolins, and A. P. Ramirez, "The materials genome initiative, the interplay of experiment, theory and computation," Current Opinion in Solid State and Materials Science **18**, 99–117 (2014).

[2]K. Butler, D. Davies, H. Cartwright, O. Isayev, and A. Walsh, "Machine learning for molecular and materials science," Nature **559**, 547–555 (2018).

[3]A. de Almeida, R. Moreira, and T. Rodrigues, "Synthetic organic chemistry driven by artificial intelligence," Nature Reviews Chemistry **3**, 589–604 (2019).

[4]N. Brown, P. Ertl, R. Lewis, T. Luksch, D. Reker, and N. Schneider, "Artificial intelligence in chemistry and drug design," Journal of Computer-Aided Molecular Design **34**, 709–715 (2020).

[5]A. O. Oliynyk, E. Antono, T. D. Sparks, L. Ghadbeigi, M. W. Gaultois, B. Meredig, and A. Mar, "High-throughput machine-learning-driven synthesis of full-heusler compounds," Chemistry of Materials **28**, 7324–7331 (2016).

[6]T. Ueno, T. D. Rhone, Z. Hou, T. Mizoguchi, and K. Tsuda, "Combo: An efficient bayesian optimization library for materials science," Materials Discovery **4**, 18–21 (2016).

[7]R. Ouyang, E. Ahmetcik, C. Carbogno, M. Scheffler, and L. M. Ghiringhelli, "Simultaneous learning of several materials properties from incomplete databases with multi-task sisso," Journal of Physics: Materials **2**, 024002 (2019).

[8]G. Pilania, J. E. Gubernatis, and T. Lookman, "Structure classification and melting temperature prediction in octet ab solids via machine learning," Physical Review B **91**, 214302 (2015).

[9]P. C. Jennings, S. Lysgaard, J. S. Hummelshøj, T. Vegge, and T. Bligaard, "Genetic algorithms for computational materials discovery accelerated by machine learning," npj Computational Materials **5**, 46 (2019).

[10]H. Matter, "Selecting optimally diverse compounds from structure databases : A validation study of two-dimensional and three-dimensional molecular descriptors," Journal of Medicinal Chemistry **40**, 1219–1229 (1997).

[11]P. R. Wiecha, "Deep learning for nano-photonic materials – the solution to everything!?" Current Opinion in Solid State and Materials Science **28**, 101129 (2024).

[12]V. Sanders, B. Asay, T. Foley, B. Tappan, A. Pacheco, and S. S.F., "Reaction propagation of four nanoscale energetic composites (al/moo3, al/wo3, al/cuo, and bi2o3)," Journal of Propulsion and Power **23**, 707–714 (2007).

[13]P. Gandhi, M. Schoenitz, and E. Dreizin, "Evaluation and design of metal-based gas-generating energetic materials," Combustion and Flame **249**, 112615 (2023).

[14]T. Wu, F. Sevely, B. Julien, F. Sodre, J. Cure, C. Tenailleau, A. Esteve, and C. Rossi, "New coordination complexes-based gas-generating energetic composites," Combustion and Flame **219**, 478–487 (2020).

[15]Y. Aly, M. Schoenitz, and E. Dreizin, "Aluminum-metal reactive composites," Combustion Science and Technology **183**, 1107–1132 (2011).

[16]H. Wang, B. Julien, D. J. Kline, Z. Alibay, M. C. Rehwoldt, C. Rossi, and M. R. Zachariah, "Probing the reaction zone of nanolaminates at s time and m spatial resolution," The Journal of Physical Chemistry C **124**, 13679–13687 (2020).

[17]M. R. Zachariah, "Nanoenergetics: Hype, reality and future," Propellants, Explosives, Pyrotechnics **38**, 7 (2013).

[18]V. Baijot, M. Djafari-Rouhani, C. Rossi, and A. Esteve, "A multi-phase micro-kinetic model for simulating aluminum based thermite reactions," Combustion and Flame **180**, 10–19 (2017).

[19]J. M. Epps, J.-P. Hickey, and J. Z. Wen, "Modelling reaction propagation for Al/CuO nanothermite pellet combustion," Combustion and Flame **229**, 111374 (2021).

[20]E. Tichtchenko, B. Bedat, O. Simonin, L. Glavier, D. Gauchard, A. Esteve, and C. Rossi, "Comprehending the influence of the particle size and stoichiometry on al/cuo thermite combustion in close bomb: A theoretical study," Propellants, Explosives, Pyrotechnics **48**, e202200334 (2023).

[21]K. M. De Souza and M. J. de Lemos, "Advanced one-dimensional modeling of thermite reaction for thermal plug and abandonment of oil wells," International Journal of Heat and Mass Transfer **205**, 123913 (2023).

[22]M. M. Islam and A. Strachan, "Role of dynamical compressive and shear loading on hotspot criticality in RDX via reactive molecular dynamics," Journal of Applied Physics **128**, 065101 (2020).

[23]E. Tichtchenko, A. Estève, and C. Rossi, "Modeling the self-propagation reaction in heterogeneous and dense media: Application to Al/CuO thermite," Combustion and Flame **228**, 173–183 (2021).

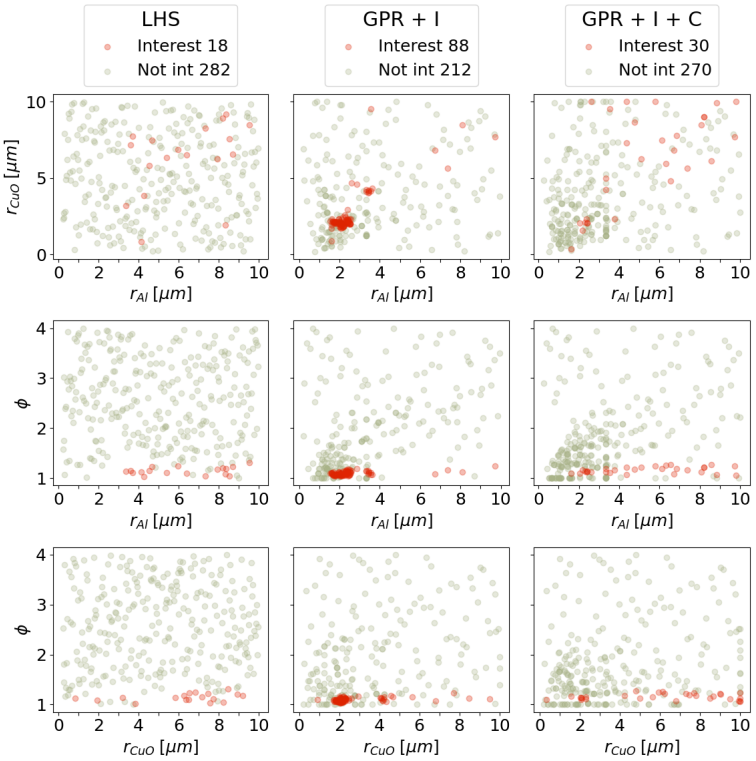

FIG. 6. Spatial distribution of the total number of sampled points (300) projected onto main feature scale planes. Red balls correspond to points of interest, while gray balls represent non-interesting points. Region of interest, R2, is defined for temperatures and pressures in the range 40-56 MPa and 5800-7000 K, respectively. "Not int" *stand for not interesting points.*

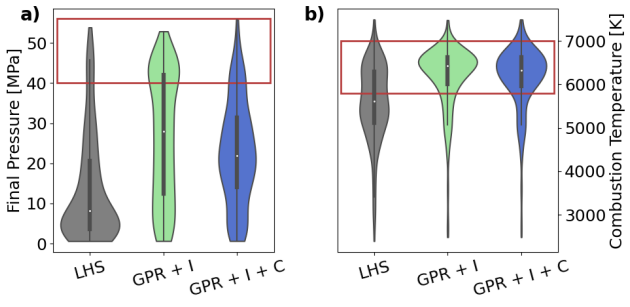

FIG. 7. Violin plots depicting the targets of the 300 Al/CuO sampled thermites obtained with LHS and each active sampling scenario. a) Final pressure, b) Combustion temperature. The red lines mark the limits of the region of interest R2.

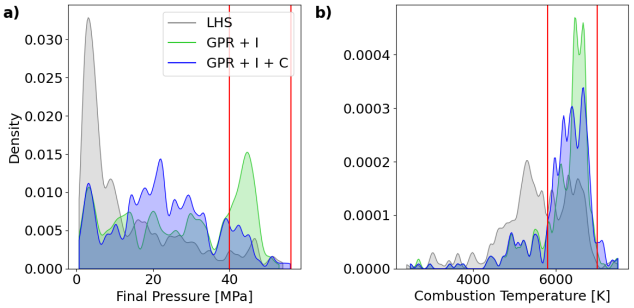

FIG. 8. KDE plots depicting the targets of the 300 Al/CuO sampled thermites obtained with LHS and each active sampling scenario. a) Final pressure, b) Combustion temperature. The red lines mark the limits of the region of interest R2.

[24] P. V. Balachandran, D. Xue, J. Theiler, J. Hogden, and T. Lookman, "Adaptive strategies for materials design using uncertainties," Scientific Reports **6**, 19660 (2016).
[25] C. C. S. Freitas, F. C. Peixoto, and A. S. Vianna, "Simulation of a thermal battery using phoenics®," Journal of Power Sources **179**, 424–429 (2008).
[26] H. Habu, M. Okada, M. Lto, K. Nozoe, T. Kawano, S. Matsumoto, and Y. Yoshida, "Thermite as a chemical heat source for the science payload," Science and Technology of Energetic Materials **73**, 147–152 (2012).
[27] N. Banerjee, Y. Xie, M. Rahman, H. Kim, and C. H. Mastrangelo, "From chips to dust: The mems shatter secure chip," in *2014 IEEE 27th International Conference on Micro Electro Mechanical Systems (MEMS)* (2014) pp. 1123–1126.
[28] F. Sevely, T. Wu, F. Sodre Ferreira, L. Seguier, V. Brossa, S. Charlot, A. Esteve, and C. Rossi, "Developing a highly responsive miniaturized security device based on a printed copper ammine energetic composite," Sensors and Actuators A: Physical **346**, 113838 (2022).
[29] T. Wu and M. R. Zachariah, "Silver ferrite: a superior oxidizer for thermite-driven biocidal nanoenergetic materials," RSC Adv. **9**, 1831–1840 (2019).
[30] T. Wu, B. Julien, H. Wang, S. Pelloquin, A. Esteve, M. R. Zachariah, and C. Rossi, "Engineered porosity-induced burn rate enhancement in dense al/cuo nanothermites," ACS Applied Energy Materials **5**, 3189–3198 (2022).

[31]V. L. Deringer, A. P. Bartók, N. Bernstein, D. M. Wilkins, M. Ceriotti, and G. Csányi, "Gaussian process regression for materials and molecules," Chemical Reviews **121**, 10073–10141 (2021).

[32]P. Virtanen, R. Gommers, T. E. Oliphant, M. Haberland, T. Reddy, D. Cournapeau, E. Burovski, P. Peterson, W. Weckesser, J. Bright, S. J. van der Walt, M. Brett, J. Wilson, K. J. Millman, N. Mayorov, A. R. J. Nelson, E. Jones, R. Kern, E. Larson, C. J. Carey, İ. Polat, Y. Feng, E. W. Moore, J. VanderPlas, D. Laxalde, J. Perktold, R. Cimrman, I. Henriksen, E. A. Quintero, C. R. Harris, A. M. Archibald, A. H. Ribeiro, F. Pedregosa, P. van Mulbregt, and SciPy 1.0 Contributors, "SciPy 1.0: Fundamental Algorithms for Scientific Computing in Python," Nature Methods **17**, 261–272 (2020).

[33]H. Wang, B. van Stein, M. Emmerich, and T. Back, "A new acquisition function for bayesian optimization based on the moment-generating function," in *2017 IEEE International Conference on Systems, Man, and Cybernetics (SMC)* (2017) pp. 507–512.

[34]G. P. Kontoudis and M. Otte, "Adaptive exploration-exploitation active learning of gaussian processes," in *2023 IEEE/RSJ International Conference on Intelligent Robots and Systems (IROS)* (2023) pp. 9448–9455.

[35]A. Nicollet, L. Salvagnac, V. Baijot, A. Estève, and C. Rossi, "Fast circuit breaker based on integration of al/cuo nanothermites," Sensors and Actuators A: Physical **273**, 249–255 (2018).

[36]"M. musy et al., "vedo, a python module for scientific analysis and visualization of 3d objects and point clouds", https://vedo.embl.es/?amp=1," (2021).

[37]E. Tichtchenko, V. Folliet, O. Simonin, B. Bédat, L. Glavier, A. Esteve, and C. Rossi, "Combustion model for thermite materials integrating explicit and coupled treatment of condensed and gas phase kinetics," Proceedings of the Combustion Institute **39**, 3637–3645 (2023).

[38]E. Tichtchenko, B. Bedat, O. Simonin, L. Glavier, D. Gauchard, A. Esteve, and C. Rossi, "Comprehending the influence of the particle size and stoichiometry on al/cuo thermite combustion in close bomb: A theoretical study," Propellants, Explosives, Pyrotechnics **48**, e202200334 (2023).